Journal of ELECTRONIC MATERIALS, Vol. 45, No. 8, 2016
DOI: 10.1007/s11664-016-4539-9

Theoretical and Experimental Exploration of Breakdown Phenomena in an Argon-Filled GaP Device

H. HILAL KURT,[1,4] EVRIM TANRIVERDI,[2] and EROL KURT[3]

1.—Department of Physics, Faculty of Science, Gazi University, Teknikokullar, 06500 Ankara, Turkey. 2.—Division of Physics, Institute of Science, Gazi University, Teknikokullar, 06500 Ankara, Turkey. 3.—Department of Electrical and Electronics Engineering, Technology Faculty, Gazi University, Teknikokullar, 06500 Ankara, Turkey. 4.—e-mail: hkurt@gazi.edu.tr

A plasma device with large diameter and short interelectrode distance has been designed and implemented. Theoretical modeling and simulations have been carried out for different interelectrode distances, and experimental results obtained under different pressures p, both with argon atmosphere. The device produces direct-current (dc) discharges in the parallel-plate electrode configuration, with gallium phosphide (GaP) semiconductor at one side and SnO_2-coated glass conducting material at the other side, separated by gas medium with width of 50 μm to 500 μm. The device can be operated under different values of interelectrode distance d, applied voltage U, and gas pressure p. Current–voltage characteristics and breakdown voltages have been found experimentally and theoretically. In addition, theoretical breakdown curves have been derived from simulations. The theory can also identify the space-charge density, thermal electron velocity, reduced electric field strength (E/N), electron density ne, and secondary-electron emission (γ). Comparison between experiment and theory shows that the theory can estimate the breakdown very well for low pressure and small interelectrode gap.

Key words: GaP semiconductor cathode, argon discharge, plasma, breakdown

INTRODUCTION

Gallium phosphide (GaP) is a III–V semiconductor, having an indirect wide bandgap (WBG) of 2.26 eV at room temperature, enabling its use in many electrical and optical applications[1,2] such as light-emitting diodes, nanosensor devices, optical limiters, and acoustooptical modulators.[1–3] According to recent research, GaP is considered an interesting material because of its potential application in terahertz-scale laser generation and detection in the wide application area of high-technology pulsed laser systems at 1040 nm;[4] For instance, GaP can be used as a good emitter for energy enhancement of terahertz pulses at very high pump powers.[5] In addition, it can be used in construction of photodetector tubes, since GaP avalanche photodiodes give high response in the wavelength range from 400 nm to 500 nm.[6]

According to discharge physics, there are two discharge modes, namely Townsend discharge (TD) and glow discharge (GD).[7] TD is a weak discharge resulting in lower space-charge generation and producing low discharge current. The external electric field E is not destroyed, and the maximum discharge light emission (DLE) radiated from excited atoms occurs in the vicinity of the metal anode.[8,9] The second type of discharge, i.e.,GD, has a strong discharge mechanism and yields high space-charge generation.[10] The positive charges are gathered near the cathode, resulting in a cathode drop, as demonstrated by the highly illuminated plane situated near the semiconductor cathode. The type of gas, pressure p, electrode structure, and discharge gap d are important system parameters determining such discharges. In most cases, the external voltage can be considered

(Received November 30, 2015; accepted April 12, 2016; published online May 19, 2016)

different from the breakdown voltage U_B. However, large numbers of electrons are created and result in electrical current before breakdown in TD.[11] According to literature, electrons can also be generated via associative ionization.[12] They can contribute to conductivity by desorption from barriers or electron emission from metastable ions.[12] According to literature, the applied voltage, which produces a current between the cathode and anode, is denoted U_B (i.e., the breakdown voltage). Based on U_B values, Paschen curves are drawn as a function of the product of p and d[11–14] to obtain the characteristic of the device.

By filling with a gas at a certain pressure p for a cathode made from a semiconductor material, and defining a microscale interelectrode distance, one can construct a microelectronic gas discharge device (MGDD), having well-known applications in microwave components based on WBG semiconductors. Because high-frequency power components are widely used in microwave devices, GaP is more appropriate than GaAs or pure Si materials in terms of trap concentration.[15,16] A recent study by Astrov et al.[17] reported oscillatory patterns on the GaAs semiconductor cathode, demonstrating complicated dynamics of the discharge phenomena in cells with small gaps. In addition, they also measured bifurcation behavior for some applied voltages in their cell, namely the discharge current showed two distinct values for one applied cell voltage. Such behavior again demonstrates the complex discharge dynamics on the semiconductor plate. Therefore, much research has been done in this direction, recently.

Herein, discharge results from a theoretical model and experiments using a new MGDD operating with argon medium are reported. The paper is organized as follows: In "Theory" section, a brief explanation on the theoretical background is presented. "Experimental Procedures" section provides the experimental details and setup. The main theoretical and experimental results and their comparison are presented in the following section. The "Conclusions" section summarizes the important highlights of the theoretical and experimental studies.

THEORY

Figure 1 presents the simulation cell. While one side of the cell is a semiconducting material, the other side is a conductor. A filling gas is present between the electrodes.

In this geometry, the following theoretical background can be applied. Initially, we start with the secondary-electron emission (SEE) process from the cathode surface as a result of the bombardment effect. This is vital as it affects the onset of the electrical discharge. According to literature, there is growing interest in generating the SEE process, concentrating on the dependence of the electron escape factor f_{esc} on gas-induced creation of ions and ultraviolet–visible photons. The energy conversion from the cathode for an incident ion can be evaluated by studying f_{esc}.[18–20] Indeed, an external field can also occur and propagate in the gas volume. Thus, the electrons lead to a certain spatiotemporal distribution below the breakdown voltage. Discharge plasma ignition has been considered theoretically under the effects of the initial secondary or volume electrons and the field itself.[21,22]

SEE attracts attention because of the important applications of such microdevices, including microelectromechanical systems, semiconductor devices, excimer sources, plasma display panels, lasers, electron multipliers, etc.[23–25] According to recent studies, the importance of emission processes from a surface and of electron-induced collisional transfer has increased in the framework of SEE; For instance, Ref. 21 showed that SEE levels for various gas media change with E/N, where E and N are the electrical field and gas density, respectively. There, the contribution of γ was found to be important for the evolution of the breakdown at high E/N values. Paschen curves have been very important for identification of SEE processes for such microplasmas.[26,27] It is known that strong dc fields support both an ion current toward the cathode and enhanced electron-induced ionization. In addition, Ref. 28 showed that, on the micrometer scale, the Paschen curve scales with the product pd and j/p^2 (where d and j are the discharge gap and current density, respectively), when only electrons are emitted by the surface with discharge bombardment. It is also observed that γ can reach remarkably higher values because of enhanced photoionization due to photons.[29–31] In this regard, excitation of filling gas atoms results in higher values for the gas as well as photon-induced SEE. In gas media, Refs. 26 and 31 proved that low ionization coefficient α/N is vital for delayed breakdown. However, SEE phenomena related to semiconductor cathodes have not yet been fully studied in terms of electrical breakdown. Indeed, the effect of γ is not exactly known for semiconductor cathodes.[32,33]

For many applications, uniform plasma distribution is required, so semiconductor cathodes are fabricated with a homogeneous spatial distribution of resistance corresponding to the onset of space charge. In fact, filament propagation is stopped by such a semiconductor cathode with high resistivity. Thus, a uniform plasma distribution is formed, resulting in a low-current microdischarge for use in the aforementioned applications.

From the applied voltage, the α/N ratio in the gas volume can be found as

$$\frac{\alpha}{N} = A e^{\left(-\frac{BN}{E}\right)} \quad (1)$$

based on the number of ionizations by an electron per unit length, with the coefficients A and B being

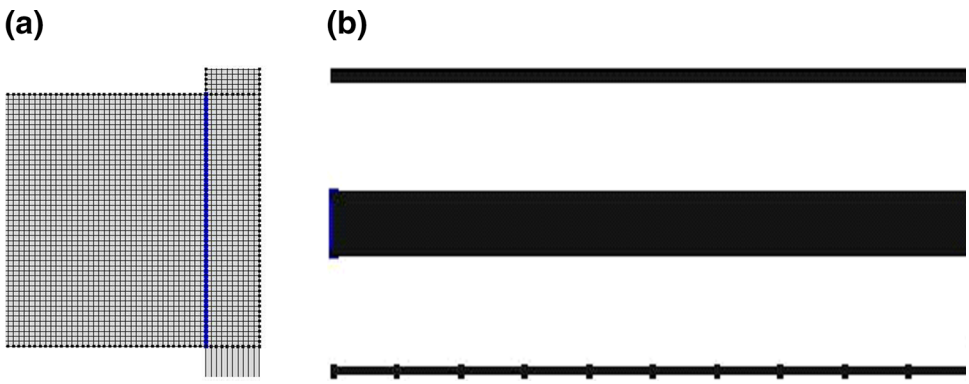

Fig. 1. Simulation cell: (a) intersection region of simulation cell, (b) dc argon plasma cell.

Table I. Physical features of cell

Parameter	Value
Diameter (D)	15 mm
Total thickness	2.5 mm
Interelectrode gap (d)	50 μm to 500 μm
Applied potential (U)	100 V to 2500 V
Filled gas pressure (p)	0.4 kPa to 101 kPa

experimental constants for the gas, which can be found using a fitting process. However, the validity of the constants A and B affects the α/N ratios for certain ranges of E/N.

Beyond this timescale, breakdown occurs, and electron multiplication sustains rapid growth of the current between the cathode and anode. Thus,

$$\gamma\left(e^{(-\alpha d)} - 1\right) = 1 \qquad (2)$$

describes the condition for ignition of self-sustaining discharge. Note that γ is the number of electrons that escape from the cathode per ion. From Eq. 2, the Townsend coefficients α and γ can be obtained as the condition for breakdown. The emission concept behind this expression is similar to that for electrons coming from the cathode as a result of ultraviolet (UV) radiation, metastable species, photons, or ions striking the cathode. However, there are several other mechanisms that result in electron emission from the cathode, including cathode heating and field-induced electron emission. The electrons emitted from the cathode also depend on ion movement.[34]

When a potential difference greater than the breakdown voltage U_B is applied to the electrodes, discharge occurs between them. Note that all simulations in this work were carried out using the Comsol Multiphysics package. The parameters of the cell are presented in Table I.

The simulations were carried out using finite-element analysis on a mesh with 42,560 elements. The system uses the gas discharge formalism as described above and the required material constants to find steady-state solutions.

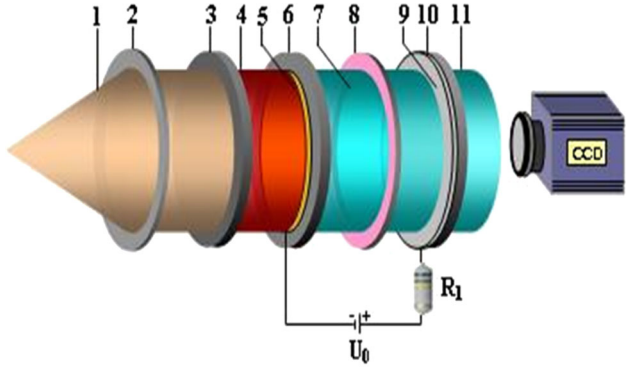

Fig. 2. Gas discharge device with GaP semiconductor cathode: 1, incident light beam; 2, lens; 3, Si filter; 4, infrared (IR) light beam; 5, semitransparent Au layer; 6, GaP semiconductor cathode; 7, gas discharge gap; 8, mica foil; 9, transparent conductive SnO_2 contact; 10, flat glass disc; 11, UV–visible light beam.

EXPERIMENTAL PROCEDURES

The experimental arrangement of the microplasma cell with GaP cathode is shown in Figs. 2 and 3.

Figure 2 shows the discharge device only. The parts of the discharge device comprise 11 elements. Note that the gas discharge gap (i.e., no. 7) can be adjusted for each experimental study. The whole measurement system is presented in Fig. 3. To sustain a voltage difference between the electrodes, a direct-current (dc) voltage of up to 2000 V is applied. Note that this can be applied gradually through the experiment. A photomultiplier is also attached to record the DLE, mainly being used for optical explorations. In addition, a Stanford PS325 digital high-power supply (2500 V, 25 W) is utilized. Experimental measurements are taken via a connection to a personal computer (PC). Note that insulating mica foil should be placed between the GaP cathode and anode to form a microscale argon-filled gap between the electrodes. The basic circuit is formed to measure the discharge current I (see

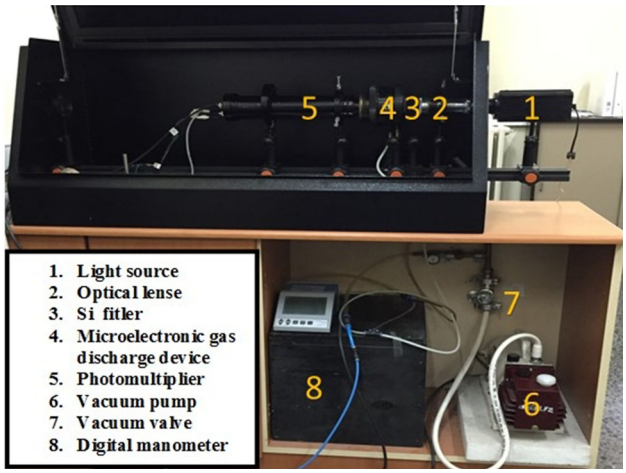

Fig. 3. Gas discharge device with GaP semiconductor cathode and measurement tools.

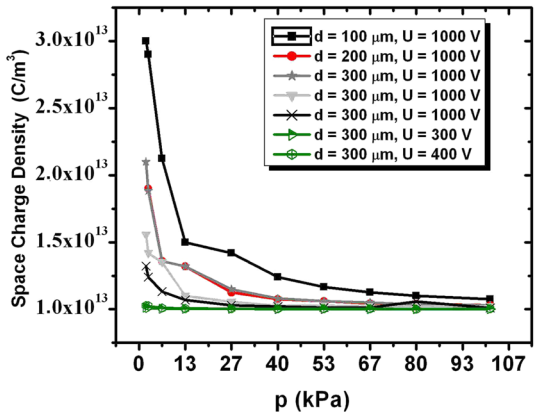

Fig. 4. Space-charge density versus gas pressure for various values of external voltage and interelectrode gap.

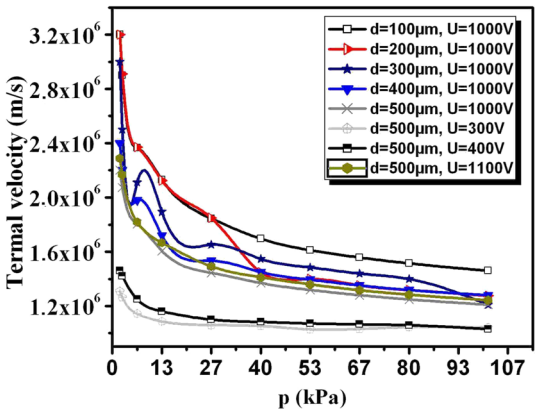

Fig. 5. Electron thermal velocity versus gas pressure for various values of potential and interelectrode gap.

Fig. 1). The interelectrode gap d and semiconductor diameter D of the GaP discharge device can be adjusted to values between 143 μm and 525 μm and 15 mm and 22 mm, respectively.

The voltage values are swept up/down between 200 V and 2500 V if there is a need to scan the whole discharge regime. In the device, the ohmic contact to the n-type GaP semiconductor is produced by the evaporation method, forming transparent Au film at about 350°C. The pressure range can be changed from 3.7 kPa to 91.7 kPa during the experiments. This also enables one to obtain the Paschen curve for the device. I can be measured using a digital multimeter (Keithley 199) through a 10-kΩ resistor connected in series to the discharge device. The gas discharge gap is located between the GaP semiconductor and a glass disc, as shown in Fig. 2. The discharge is produced between these two electrodes. The current–voltage characteristics of the GaP cathode can be measured at room temperature, and the current–voltage characteristics (CVCs) recorded for external voltages with increasing/decreasing rate of 5 V/s. The photocathode in the device can also be illuminated using an incandescent lamp. However, in the present study only results in the dark are presented.

RESULTS AND DISCUSSION

Theoretical Results

According to the theoretical simulations, the physical parameters of the cell play an important role in determining the charge density, electron thermal velocity, and secondary-electron emission distribution. Figure 4 presents the electron charge density for various pressure values. It is obvious that increase in p decreases the charge density within the gap of the cell. Beyond 13.3 kPa, the charge density ρ decreases to 1×10^{13} C/m^3. Thus, it is clear that the charge density decreases at least threefold beyond a certain pressure value.

Specifically, the charge density goes up to $\rho = 3 \times 10^{13}$ C/m^3 for an interelectrode gap $d = 500$ μm and $U = 1000$ V. However, the density decreases as d is decreased. In addition, lower applied voltage U results in lower charge density.

Figure 5 presents the results for the thermal velocity at various pressure values. The velocity can take a value $v = 3 \times 10^6$ m/s at lower pressures, in agreement with literature. However, the velocity decreases to 1.5×10^6 m/s beyond 33.25 kPa. The particles in the gas can move easily at low pressure, due to the substantial decrease in collisions among them.

In general, increasing the gap causes a decrease in velocity. This is also related to the fact that the interaction with gas particles causes successive collisions that substantially decrease the velocity. Figure 6a and b shows the electron density for various pressure values. It is obvious that the electron densities are similar, except for one case (i.e., $d = 500$ μm and $U = 1000$ V). The reason for this high number density could be high ionization rates in the gas medium. The density has a highest

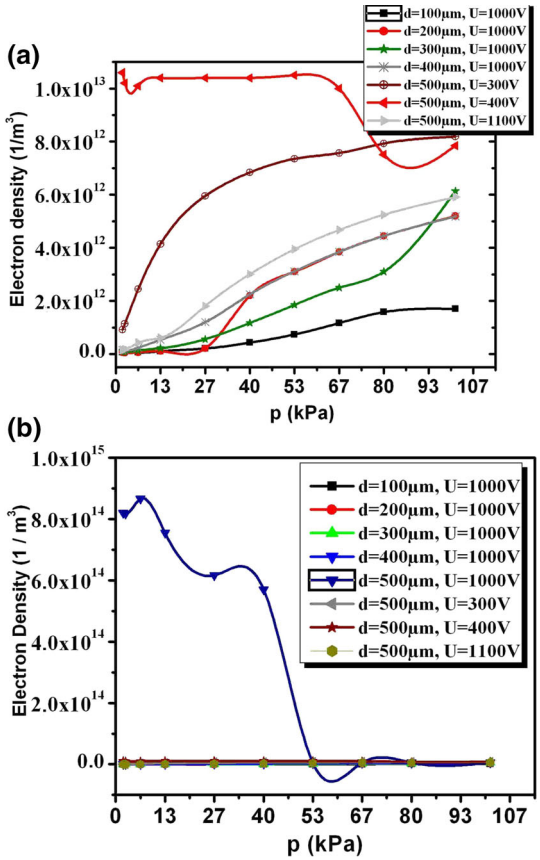

Fig. 6. Electron density versus gas pressure. Note that (a) shows the lower part of (b).

value of 8.5×10^{15} m^{-3}, decreasing dramatically beyond 6.65 kPa (Fig. 6a).

Note also that this highest density becomes similar to the other densities at 53 kPa, as clearly seen in Fig. 6b. The electron density is around 6×10^{12} m^{-3}. In addition, the electron number density increases with the interelectrode gap for the same p value.

Secondary-electron emission curves are shown in Fig. 7. Initially, comparing Fig. 6a with Fig. 7, it can be stated that secondary emission does not play any role, since the maximal density case (i.e., U = 1000 V and d = 500 μm) has the lowest secondary emission for the same pressure value. Therefore, one can state that the contribution of secondary emission to the electron density is not important for the discharge mechanism.

According to Fig. 7, the maximal secondary-emission peaks occur at 26.6 kPa in the cases of (U, d) = (1000 V, 200 μm) and (U, d) = (1000 V, 100 μm). Thus, it can be concluded that secondary emission dominates at lower interelectrode gap but higher voltage values.

Figure 8 presents the Paschen curves for d = 50 μm, d = 100 μm, and d = 525 μm. According to the results of the theoretical study, the breakdown threshold is found to be U_B = 373 V at d = 525 μm.

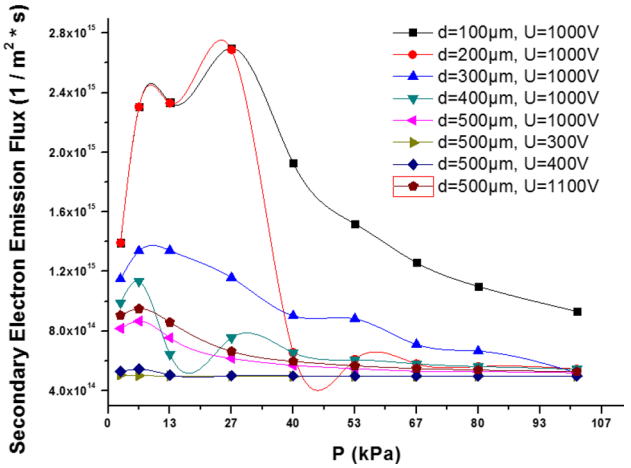

Fig. 7. Secondary-electron emission versus gas pressure for various values of interelectrode gap and applied voltage.

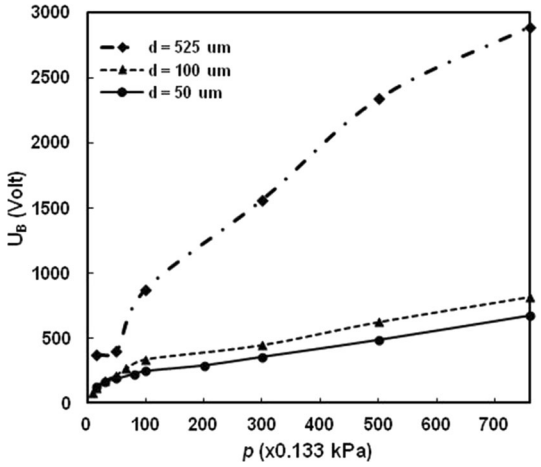

Fig. 8. Theoretical Paschen curve for different interelectrode gaps d at D = 15 mm.

Moreover, it decreases to U_B = 264 V and U_B = 225 V for gaps of 100 μm and 50 μm, respectively. It will be shown that all these values are in good agreement with the experimental findings below. This curve gives the lowest voltage value that will sustain a measurable current flow between the electrodes. When the experimental breakdown voltage is adjusted to the theoretical results for the same pressure, an electron density of 7620 mA/m^2 is found for the simulated cell. This value is used as a condition for breakdown ignition. Then, the entire curves are plotted based on these findings, using the different distance and pressure values. Note also that the electrode shape, interelectrode gap, and type of gas also play important roles in determining the threshold value of the Paschen curve. In addition, the discharge coefficient and ionization coefficient should be known for better theoretical estimations. It should also be noted that theory cannot predict the breakdown values at high pressure; For instance,

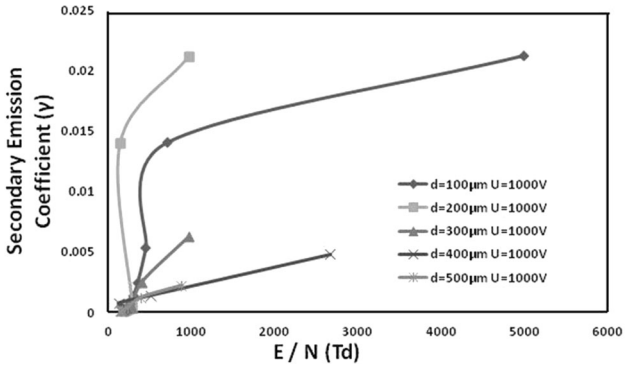

Fig. 9. γ coefficient for increasing Td (1 $Td = 10^{-21}$ V m^2).

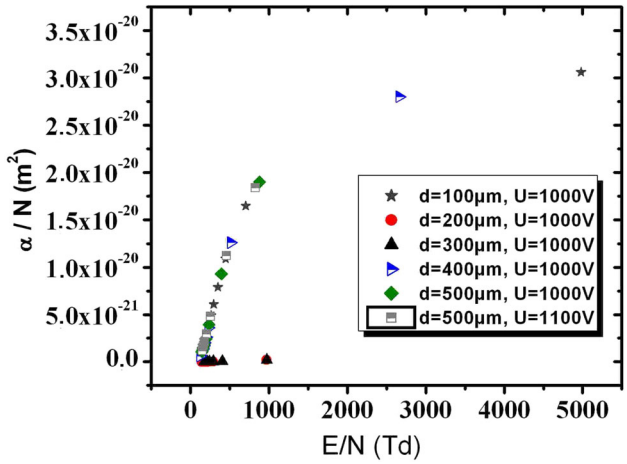

Fig. 10. Coefficient α/N versus E/N (1 $Td = 10^{-21}$ V m^2).

with d = 525 μm and p = 66.5 kPa, the experimental breakdown results give U_B = 982 V, while the theory gives a much higher value of 2341 V for the same parameter values. Thus, this theoretical model can only work for low pressure. For the second gap value (i.e., d = 100 μm), breakdown occurs theoretically at 622 V for p = 66.5 kPa. However, the experiments gave 499 V for the same pressure value. Similarly, the theoretical and experimental breakdown values are 487 V and 360 V for d = 50 μm. It can also be concluded that the agreement with the model improves as the interelectrode gap decreases. Therefore, we believe that the effects of the gas coefficient and ionization events play an important role in breakdown estimation for large gaps.

Figure 9 shows the coefficient γ for the product Td. It was found that γ takes values up to 0.02. Note also that it exhibits a decreasing trend with increasing E field, as in literature.

Townsend discharge is a gas ionization process. Therefore, free electrons are accelerated by the strong E field. This process gives rise to electrical conduction through avalanche multiplication inside the gas. At this point, one should consider ionization of molecules. When the number of free charges

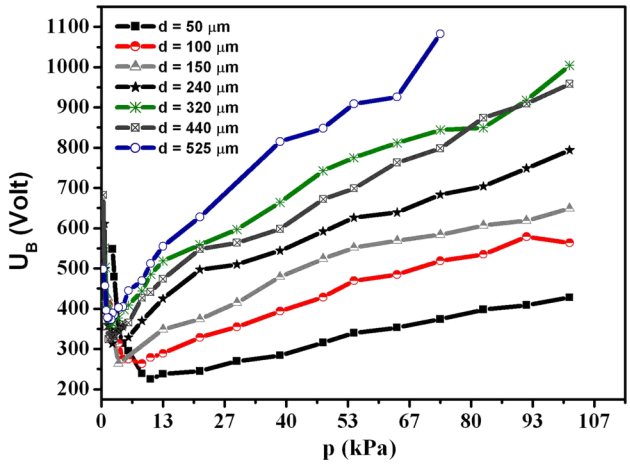

Fig. 11. Experimental Paschen curves for various interelectrode gaps at D = 15 mm.

drops or the electric field weakens, the process stops. Note also that 1 Td has a value of 10^{-21} V m^2.

Figure 10 shows the coefficient α/N versus E/N. It is obvious that there are two distinct regimes. One has relatively higher coefficient α/N, whereas the other has too low a coefficient. Basically, low coefficient values are obtained at 200 μm and 300 μm. The field causes the coefficient to increase in general up to 3 $\times$ 10^{-20}.

As in earlier studies,[35,36] these coefficients show different curves for various interelectrode gaps. It is obvious that larger gaps result in higher coefficient values in general. Note also that the slope of the coefficient curves decreases slightly versus E/N.

Experimental Results

In this section, experimental Paschen curves are presented for various interelectrode gaps from 50 μm to 525 μm (Fig. 11). Note that all the results were measured for cathode diameter D = 15 mm, as in the simulations. At first glance, it is understood that the breakdown voltage increases with the gap, since the induced current requires a much greater potential difference to sustain a connection between the electrodes, as usual. It is also interesting that the pressure at which the breakdown event takes place moves towards higher values with decreasing gap. Specifically, the breakdown voltage U_B = 225 V occurs at p = 10.6 kPa in the case of d = 50 μm, whereas U_B = 378 V occurs at p = 1.6 kPa in the case of d = 525 μm. Thus, the increase with the interelectrode gap is obvious experimentally. As in all other Paschen curves, for higher p values, the discharge thresholds increase due to the large number of gas molecules. Besides, when d becomes larger, higher voltages are required for ignition of the discharge between the electrodes, as also stated in previous studies.[13,14] In addition, the slope of the curves is also important, in the sense that it increases for greater interelectrode gap. Thus, this

also proves that increase in the volume of filling gas negatively affects the discharge.

At the left-hand side of the curves, there exists another difficulty for electrical discharge, since there is insufficient conducting medium to transfer electrons from the cathode to anode, thus requiring higher potential to ignite a discharge. Therefore, pressures below 1.6 kPa are not convenient for the discharge process with GaP.

According to the theoretical and experimental findings, it is observed that the theoretical breakdown curves are in good agreement with the experimental results. While the U_B of the experiments is 378 V for d = 525 μm, the simulations give U_B = 373 V, in good agreement for the same interelectrode gap. For higher cell pressures such as 40 kPa, breakdown is observed experimentally at U_B = 824 V, whereas it is U_B = 1563 V theoretical. In the case of d = 100 μm, while the experimental study gives U_B = 263 at p = 8.65 kPa, the theory gives U_B = 264 V at the same pressure. These values are also very close to one another. In the case of d = 50 μm, the experimental breakdown curve in Fig. 11 gives U_B = 234 V at p = 10.8 kPa, whereas the theoretical findings in Fig. 8 give a value of U_B = 225 V, also close to the experimental findings. Thus, the new model can exactly estimate the breakdown value for GaP specimens in microelectronic gas discharge devices; however, it can give a rough idea of the breakdown voltage when the pressure is increased further. The reason may be the difference between the real gas discharge coefficients and the theoretical model. However, the model could be improved further by renewing the mesh structure and using the same empirical constants A and B.

In Fig. 12a and b, experimental CVCs are given. Note that these curves give the breakdown values where finite current values initially appear. To determine the breakdown for any parameter set, the applied voltage should be increased gradually; For instance, in the case of d = 100 μm, breakdown occurs at U_B = 263 V (see Fig. 12a). In the case of d = 440 μm, the breakdown value is seen to be 336 V. While Fig. 12a gives the breakdown and CVC findings for low pressure such as 2 kPa, Fig. 12b gives the breakdown and CVC data for higher pressure such as p = 101 kPa. Comparing these two figures, it is obvious that increase of the pressure suppresses discharge up to 800 V. This is similar to the Paschen curves in that the presence of many gas atoms prevents discharge between the electrodes, since successive interactions of electrons with gas atoms prevent breakdown ignition. Thus, this regime (Fig. 12b) corresponds to the right-hand side of the Paschen curves in Fig. 11. Note that increase in the interelectrode gap delays the breakdown phenomena, as usual, due to the decrease in electrical field.

In addition, one point that should also be underlined is that the stability of the CVC is obvious in

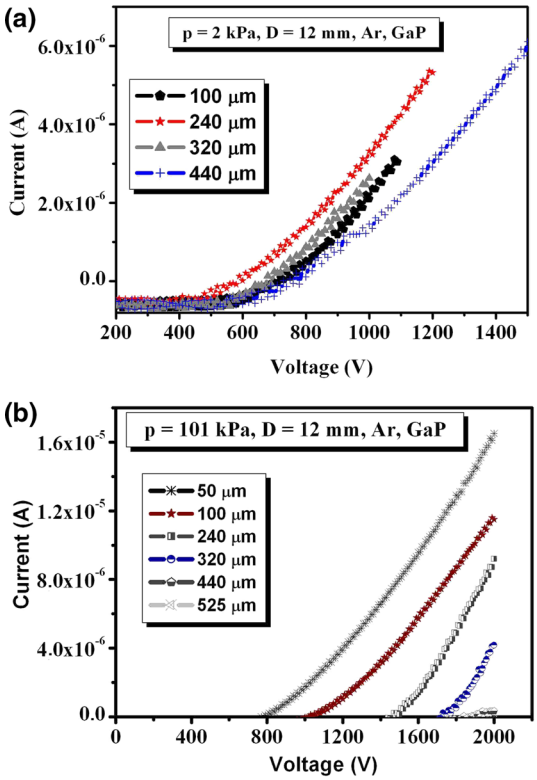

Fig. 12. Representative CVCs for various applied voltages in the cases of (a) 2 kPa and (b) 101 kPa.

the high-pressure regime (i.e., Fig. 12b), since the curves exhibit well-defined increasing trends after breakdown without any fluctuation in the current form. However, in the case of low pressure (i.e., p = 2 kPa), the CVC curves can have different values as in Fig. 12a. Thus, the stability decreases at low pressures in Ar medium.

CONCLUSIONS

Theoretical and experimental studies of a new MGDD were carried out. It has GaP semiconductor as the cathode, whereas the anode is made of a conductor. The system shows a variety of different Paschen curves, which define the starting point of the discharge. While breakdown can start at higher voltages for larger interelectrode gap, the threshold decreases to U_B = 239 V for smaller gaps. Comparison between theory and experiment shows reasonably good agreement, so the simulation could be used to predict the breakdown process of a real MGDD. Since the theoretical procedure includes the filling gas pressure and semiconductor type, the accuracy of the prediction is good. Use of such a theoretical method can reduce the costs of cell construction, as well as time consumption. Besides, coefficients such as the secondary-electron emission γ, thermal velocity, and electron density can also be found by using the theoretical model. Since the cell gap is microscale, it is not possible to measure these coefficients experimentally. Thus, the new method

is very valuable to determine system characteristics, plasma diagnostics, and Paschen curves.

ACKNOWLEDGEMENTS

This research was funded by Grants BAP Nos. 05/2012-47 and 05/2012-72 from the Gazi University Scientific Research Project Unit.

REFERENCES

1. H.W. Seo, S.Y. Bae, J. Park, H. Yang, M. Kang, S. Kim, J.C. Park, and S.Y. Lee, *Appl. Phys. Lett* 82, 3752 (2003).
2. I. Fuss and D. Smart, *Appl. Opt.* 30, 4526 (1991).
3. Z.G. Chen, L. Cheng, G.Q.M. Lu, and J. Zou, *Nanotechnology* 21, 375701 (2010).
4. Q. Wu and X. Zhang, *Appl. Phys. Lett.* 70, 1784 (1997).
5. F. Liu, Y.J. Song, Q.R. Xing, M.L. Hu, Y.F. Li, C.L. Wang, L. Chai, W.L. Zhang, A.M. Zheltikov, and C.Y. Wang, *IEEE Photon. Technol. Lett.* 22, 814 (2010).
6. D. McIntosh, Q.G. Zhou, F.J. Lara, J. Landers, and J.C. Campbell, *IEEE Photon. Technol. Lett.* 23, 878 (2011).
7. Yu.P. Raizer, *Gas Discharge Physics* (Berlin: Springer, 1991), p. 449.
8. H. Luo, Z. Liang, B. Lv, X. Wang, Z. Guan, and L. Wang, *Appl. Phys. Lett.* 91, 221504 (2007).
9. H. Yucel Kurt, E. Kurt, and B.G. Salamov, *Cryst. Res. Technol.* 39, 743 (2004).
10. M.S. Mokrov and Yu.P. Raizer, *Plasma Sources Sci. Technol.* 17, 035031 (2008).
11. Yu.B. Golubovskii, V.A. Maiorov, P. Li, and M. Lindmayer, *J. Phys. D* 39, 1574 (2006).
12. N. Gherardi, E. Croquesel, N. Naude, P. Veis, and F. Massines, *Proceedings of the 8th International Symposium on High Pressure Low Temperature Plasma Chemistry (HAKONE VIII)* (Puhajarve, Estonia, 2002).
13. E. Kurt, H. Kurt, and U. Bayhan, *Cent. Eur. J. Phys.* 7, 123 (2009).
14. H. Kurt, S. Cetin, and B.G. Salamov, *IEEE Trans. Plasma Sci.* 39, 1086 (2011).
15. O. Noblanc, C. Arnodo, C. Dua, E. Chartier, and C. Brylinski, *Mater. Sci. Forum* 338, 1247 (2000).
16. V.V. Buniatyan and V.M. Aroutiounian, *J. Phys. D* (2007). doi:10.1088/0022-3727/40/20/S18.
17. Yu.A. Astrov, A.N. Lodygin, and L.M. Portsel, *Phys. Rev. E* 91, 032909 (2015).
18. L. Schwaederle, M.K. Kulsreshath, L.J. Overzet, P. Lefaucheux, T. Tillocher, and R. Dussart, *J. Phys. D* 45, 065201 (2012).
19. M. Klas, S. Matejcik, B. Radjenovic, and M.R. Radjenovic, *Phys. Scr.* 83, 045503 (2011).
20. T.G. Rogers, A.A. Neuber, K. Frank, G.R. Laity, and J.C. Dickens, *IEEE Trans. Plasma Sci.* 38, 2764 (2010).
21. A.V. Phelps and Z.Lj. Petrovic, *Plasma Sources Sci. Technol.* 8, R21 (1999).
22. L.E. Kline and J.G. Siambis, *Phys. Rev. A* 5, 794 (1972).
23. M. Kaku, Y. Sato, and S. Kubodera, *Appl. Phys. B* 107, 85 (2012).
24. L. Schwaederlé, M.K. Kulsreshath, L.J. Overzet, P. Lefaucheux, T. Tillocher, and R. Dussart, *J. Phys. D* 45, 065201 (2012).
25. C.H. Chen, J.A. Yeh, and P.J. Wang, *J. Micromech. Microeng.* 16, 1366 (2006).
26. D. Mariotti, J.A. McLaughlin, and P. Maguire, *Plasma Sources Sci. Technol.* 13, 207 (2004).
27. H.B. Smith, C. Charles, and R.W. Boswell, *Phys. Plasmas* 10, 875 (2003).
28. Z.Lj. Petrovic, N. Skoro, D. Maric, C.M.O. Mahony, P.D. Maguire, M.R. Radenovic, and G. Malovic, *J. Phys. D* 41, 194002 (2008).
29. V.I. Gibalov and G.J. Pietsch, *Plasma Sources Sci. Technol.* 21, 024010 (2012).
30. M. Krüger, M. Schenk, M. Förster, and P. Hommelhoff, *J. Phys. B* 45, 074006 (2012).
31. M.M. Nudnova and A.Yu. Starikovskii, *J. Phys. D* 41, 234003 (2008).
32. B.G. Salamov, *J. Phys. D* 37, 2496 (2004).
33. G.G. Raju, *Gaseous Electronics* (Boca Raton: Taylor & Francis, 2006), p. 93.
34. H.Y. Kurt and E. Kurt, *Elektronika ir Elektrotechnika* 20, 1392 (2014).
35. B.G. Salamov, *J. Phys. D* 37, 2496 (2004).
36. E. Koc, S. Karaköse, and B.G. Salamov, *Phys. Status Solidi A* 210, 1806 (2013).